Electronic Supplementary Material (ESI) for Journal of Materials Chemistry C.

Electronic Supplementary Information for

Self-recovery ultraviolet-sensitive photochromic naphthalenediimide based coordination networks: Rapid fluorescence recognition of p-substituted nitrobenzenes

Zi-Xin You[†], Guang Zeng[§], Feng-Ying Bai[†], and Yong-Heng Xing[*, †]*

† College of Chemistry and Chemical Engineering, Liaoning Normal University, Dalian City, 116029, P.R. China

§ State Key Laboratory of Catalysis, Dalian Institute of Chemical and Physics, Chinese Academy of Sciences, Zhongshan Road 457, Dalian City, 116023, P.R. China

Table of Contents

Experimental Detail

Materials

All starting materials used in the experiments were without further purification (J&K Scientific, Beijing, China). N, N'-bis(carboxymethyl)-1,4,5,8-naphthalenediimide (H_2CMNDI) was synthesized by the reported method.

Instruments and measurements

Attenuated Total Reflection Infrared (ATR-IR) spectra were obtained using Nicolet iS50 FT-IR spectrometer (Thermo Fisher Scientific, Shanghai, China) with ATR-intermediate infrared module. The Perkin-Elmer 240C automatic analyzer (Perkin-Elmer, Waltham, USA) was used for the elemental analyses. Powder X-ray diffraction (PXRD) measurements were performed on a Bruker Advance-D8 X-ray powder diffractometer (Bruker, Karlsruhe, Germany) with Cu Kα radiation with a step size of 0.02° (2θ) and an acquisition time of 2 s per step in the range of 5° <2θ< 55°. Simulated PXRD patterns were obtained by single crystal data and diffraction crystal module of the Mercury program via http://www.ccdc.cam.ac.uk/mercury/[1]. Thermogravimetric (TG) analysis of sample was carried out on a Perkin Elmer Diamond TG/DTA (Perkin-Elmer, Waltham, USA) at a heating rate of 10 °C/min in N_2 or air atmosphere with the range of 20~800 °C. The N_2 adsorption–desorption isotherms, specific surface area, the pore volume and the pore size were conducted using the Autosorb-IQ-XR Gas Sorption Analyzer (Quantachrome, Florida, USA) with the Brunauer–Emmet–Teller (BET) method and the Barrett–Joyner–Halenda (BJH) method at the liquid nitrogen temperature, respectively. Cary 300 Ultraviolet-visible Spectrophotometer (Agilent, California, USA) was employed to record the UV-vis spectra (200~800 nm, for solid sample). The EPR spectra were measured on Bruker A200 Electron Paramagnetic Resonance spectrometer (Bruker, Karlsruhe, Germany). The emission spectra

were obtained by Fluoromax-4-TCSPC spectrofluorometer (HORIBA Scientific, Piscataway, USA) with Spectra LED Pulsed LED sources at room temperature (200~800 nm). Asylum Research Cypher ES AFM (Oxford Instruments, Santa Barbara, USA) was employed for atomic force microscopy (AFM) images by tapping mode.

X-ray crystallographic determination

The single crystal diffraction data were collected on a Bruker AXS SMART APEX II CCD diffractometer graphite monochromatized Mo Kα radiation (λ = 0.71073 Å) at 293 K. The data of H_2CMNDI and TM-CMNDI were solved by direct methods using SHELXTL software package[2], and refined with full matrix least-squares technique. The non-hydrogen atoms were refined with anisotropic displacement parameters. The structures were checked by PLATON program[3].

General synthesis of H_2CMNDI

2.6820 g (10 mol) 1,4,5,8-naphthalenetetracarboxylic dianhydride and 1.5019 g (20 mol) glycine were prepared and dispersed into 150 mL propionic acid, and the yellow suspension was transferred to 250 mL flasks and refluxed for 12 h. After cooled down to room temperature, the mix was washed with ethanol for several times, and the yellow product was obtained by vacuum filtration and vacuum drying. ^{1}H NMR (400 MHz, DMSO-d6): δ = 4.78 (s, 4H), 8.74 (s, 4H), 13.17 (s, 2H).

Single crystal synthesis of H_2CMNDI

0.02 g H_2CMNDI was dissolved in 1.5 mL N,N-dimethylacetamide (DMA) and 0.5 mL H_2O, and the solution was stirred for 30 min. Then 0.002 g barium chloride was added into the solution, and the mix was sttirred for 10 min, then added 50 μL 8M HNO_3. The solution was

transferred to a Pyrex glass bottle and heated in 90 °C for 2 d, and the yellow crystal was obtained.

Fluorescence sensing experiment

The samples were dispersed into the solvent in 0.2 mg/mL ratio, and the suspension carried on a ultrasonic treatment for 30 minutes. And 3 mL suspension was put into a cuvette, later, the analytes were added in a certain gradient. For the cycle experiment, the fluorescent sensor was centrifuged in 8000 r/min after each detection, and the sensor was washed by the solvent for three times, and dried in a vacuum oven.

Calculation methods

All the calculations were performed with Gaussian 09 package[4]. The B3LYP hybrid functional was employed. The 6-31g* basis set was used for the C, H, O, and N atoms. The structures of CMNDI, CMNDI radical anion (CMNDI*), and analytes were optimized and their highest occupied molecular orbitals (HOMO) and lowest unoccupied molecular orbitals (LUMO) energy levels were calculated according to the density functional theory.

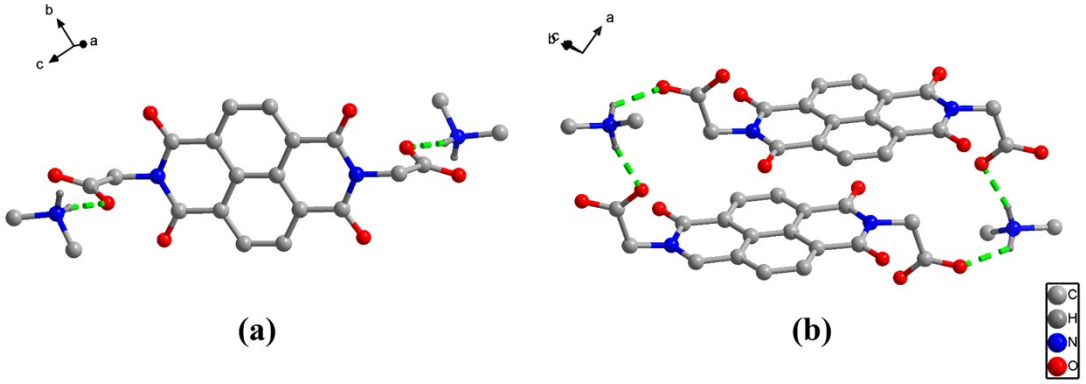

Figure S1. Molecular structure (a) and the hydrogen-bonding interaction (b) of H_2CMNDI.

Table S1. Crystallographic information of CNs*.

CNs	Co-CMNDI	Ni-CMNDI	Cu-CMNDI
Formula	$C_{18}H_{16}N_2O_{12}Co$	$C_{18}H_{16}N_2O_{12}Ni$	$C_{18}H_{16}N_2O_{12}Cu$
M ($g \cdot mol^{-1}$)	511.26	511.04	515.87
Crystal system	*Triclinic*	*Triclinic*	*Triclinic*
Space group	$P\bar{1}$	$P\bar{1}$	$P\bar{1}$
a (Å)	5.0506(6)	5.0205(4)	4.9839(5)
b (Å)	6.3217(6)	6.3112(5)	6.4217(6)
c (Å)	15.1500(16)	15.0941(13)	15.1325(14)
α (°)	95.321(4)	95.2790(10)	93.911(2)
β (°)	95.049(3)	95.0440(10)	94.548(2)
γ (°)	105.252(3)	105.1340(10)	106.073(2)
V ($Å^3$)	461.47(9)	456.59(6)	461.86(8)
Z	1	1	1
D_c ($g \cdot cm^{-3}$)	1.840	1.859	1.855
F(000)	261	262	263
M(Mo Kα) (mm^{-1})	1.009	1.142	1.261
θ (°)	1.36-24.99	2.73-24.99	1.36-27.85
Reflections collected	2389	2360	2920
Independent reflections($I>2\sigma(I)$)	1616(1443)	1605(1507)	2106(1902)
Parameters	151	151	151
Δ(ρ)(e $Å^{-3}$)	0.380&-0.421	0.401&-0.482	0.634&-0.649
Goodness of fit on F^2	1.079	1.060	1.063
R[a]	0.0399(0.0479)[b]	0.0356(0.0381)[b]	0.0478(0.0546)[b]
wR_2[a]	0.0854(0.0942)[b]	0.0908(0.0921)[b]	0.1088(0.1189)[b]

*[a]$R=\sum \left| F_O-F_C \right| / \sum \left| F_O \right|$, $wR_2=\{\sum[w(F_O^2-F_C^2)^2]/\sum[w(F_O^2)^2]\}^{1/2}$; $[F_O>4\sigma(F_O)]$. [b]Based on all data.

Table S2. Selected bond lengths (Å) and angles (°) of CNs*.

Co-CMNDI		Ni-CMNDI		Cu-CMNDI	
Co(1)-O(1)	2.183(3)	Ni(1)-O(1)	2.017(2)	Cu(1)-O(1)	1.941(3)
Co(1)-O(1)$^{\#1}$	2.183(3)	Ni(1)-O(1)$^{\#1}$	2.017(2)	Cu(1)-O(1)$^{\#1}$	1.941(3)
Co(1)-O(2)	2.046(3)	Ni(1)-O(2)	2.133(2)	Cu(1)-O(2)	2.408(3)
Co(1)-O(2)$^{\#1}$	2.046(3)	Ni(1)-O(2)$^{\#1}$	2.133(2)	Cu(1)-O(2)$^{\#1}$	2.408(3)
Co(1)-O(3)	2.094(2)	Ni(1)-O(3)	2.0601(2)	Cu(1)-O(3)	1.988(2)
Co(1)-O(3)$^{\#1}$	2.094(2)	Ni(1)-O(3)$^{\#1}$	2.0602(2)	Cu(1)-O(3)$^{\#1}$	1.988(2)

*Symmetry codes: Co-CMNDI: #1 -x+1, -y, -z+2; Ni-CMNDI: #1 -x+1, -y+1, -z; Cu-CMNDI: #1 -x+1, -y+1, -z+1.

Table S3. Bond lengths (Å) and angles (°) of hydrogen-bonding in CNs*.

Co-CMNDI				
D-H···A	d(D-H)	d(H···A)	d(D···A)	<(DHA)
O1-H1B···O6$^{\#3}$	0.85	2.00	2.833(4)	165
O2-H2D···O1$^{\#4}$	0.85	2.42	2.957(4)	121
O2-H2D···O3$^{\#4}$	0.85	2.20	2.994(4)	155
Ni-CMNDI				
D-H···A	d(D-H)	d(H···A)	d(D···A)	<(DHA)
O1-H1A···O2$^{\#3}$	0.85	2.14	2.954(3)	159
O2-H2A···O3$^{\#4}$	0.85	2.51	3.033(4)	120
Cu-CMNDI				
D-H···A	d(D-H)	d(H···A)	d(D···A)	<(DHA)
O2-H1C···O5$^{\#4}$	0.85	2.02	2.848(5)	163
O2-H2D···O1$^{\#5}$	0.85	2.17	2.816(4)	132
O2-H2D···O3$^{\#6}$	0.85	2.43	3.196(5)	151
H_2CMNDI				
D-H···A	d(D-H)	d(H···A)	d(D···A)	<(DHA)
N2-H2C···O2	0.89	1.89	2.7572(18)	164
N2-H2D···O1$^{\#1}$	0.89	2.20	2.8761(19)	132

*Symmetry codes: Co-CMNDI: #3 -x+1, -y, -z+1; #4 -x+2, -y, -z+2; Ni-CMNDI: #3 -x+2, -y+1, -z; #4 x+1, y, z; Cu-CMNDI: #4 x, y-1, z; #5 x+1, y, z; #6 –x+2, -y+1, -z+1; H_2CMNDI: #1 -1+x, y, z.

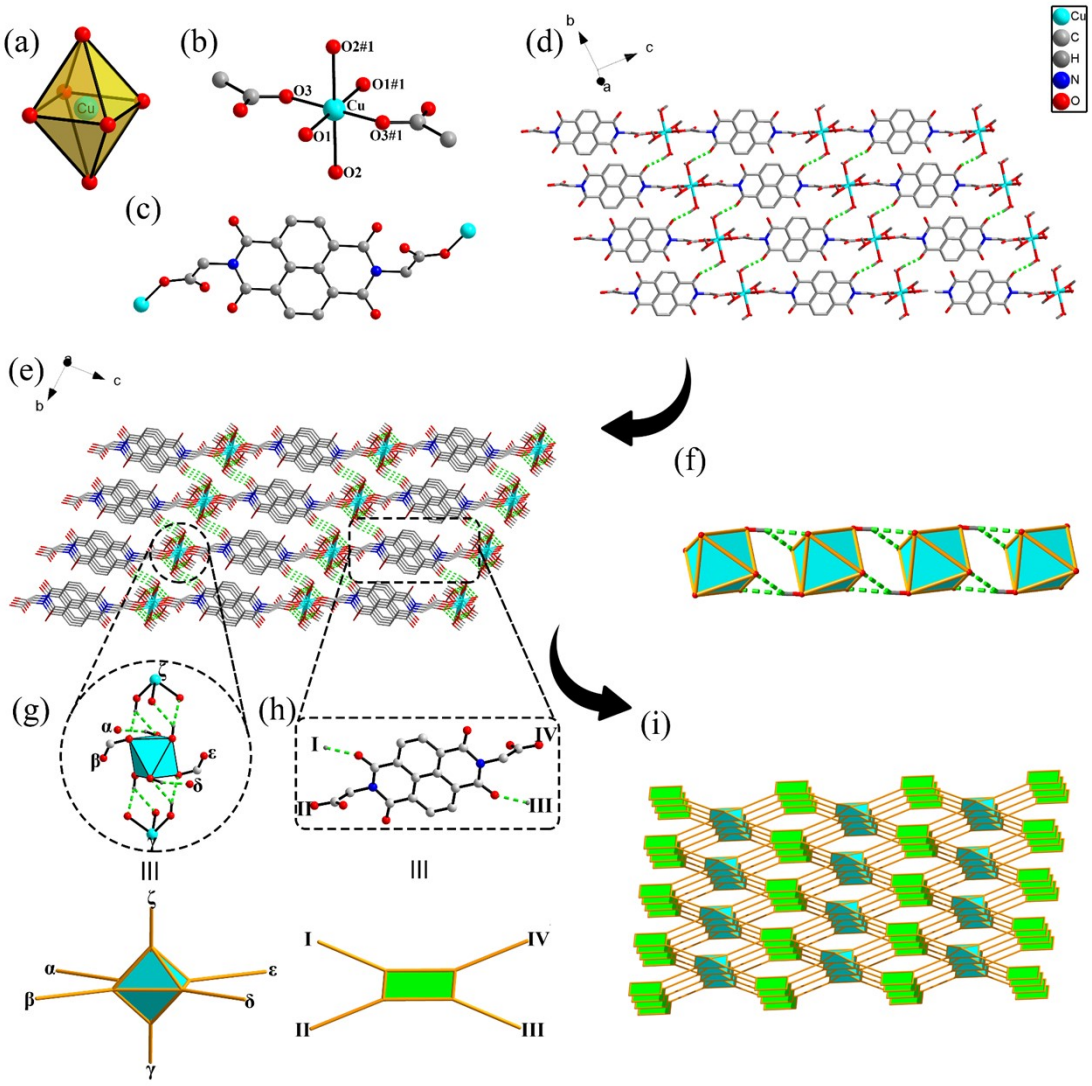

Figure S2. Structure of Cu-CMNDI: (a) Spatial configuration of Cu-O polyhedron. (b) Coordination environment of Cu(II). (c) Connection of CMNDI. (#1 -x+1, -y+1, -z+1) (d) 2D network on bc plane, the hydrogen-bonding is represented by dotted lines. (e) 3D supramolecular network. (f) Hydrogen-bonding along a direction. (g) 6-c metal node. (h) 4-c CMNDI node. (i) The underlying **fsc** net.

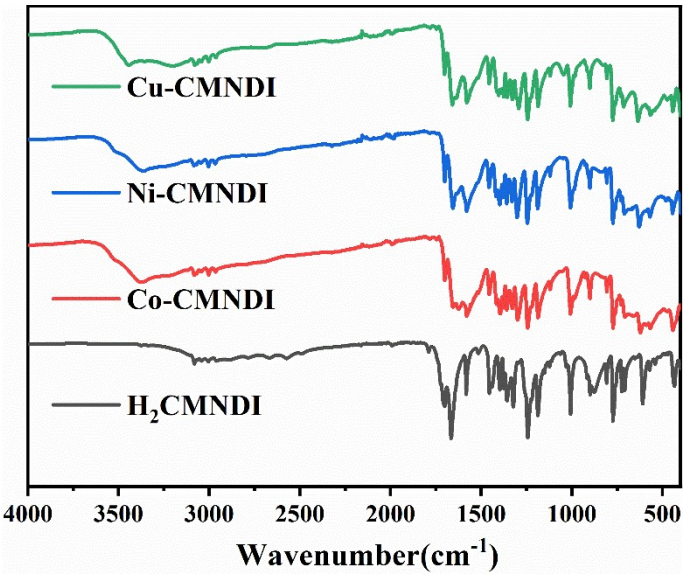

Figure S3. ATR-IR spectra of H_2CMNDI, Co-CMNDI, Ni-CMNDI, and Cu-CMNDI.

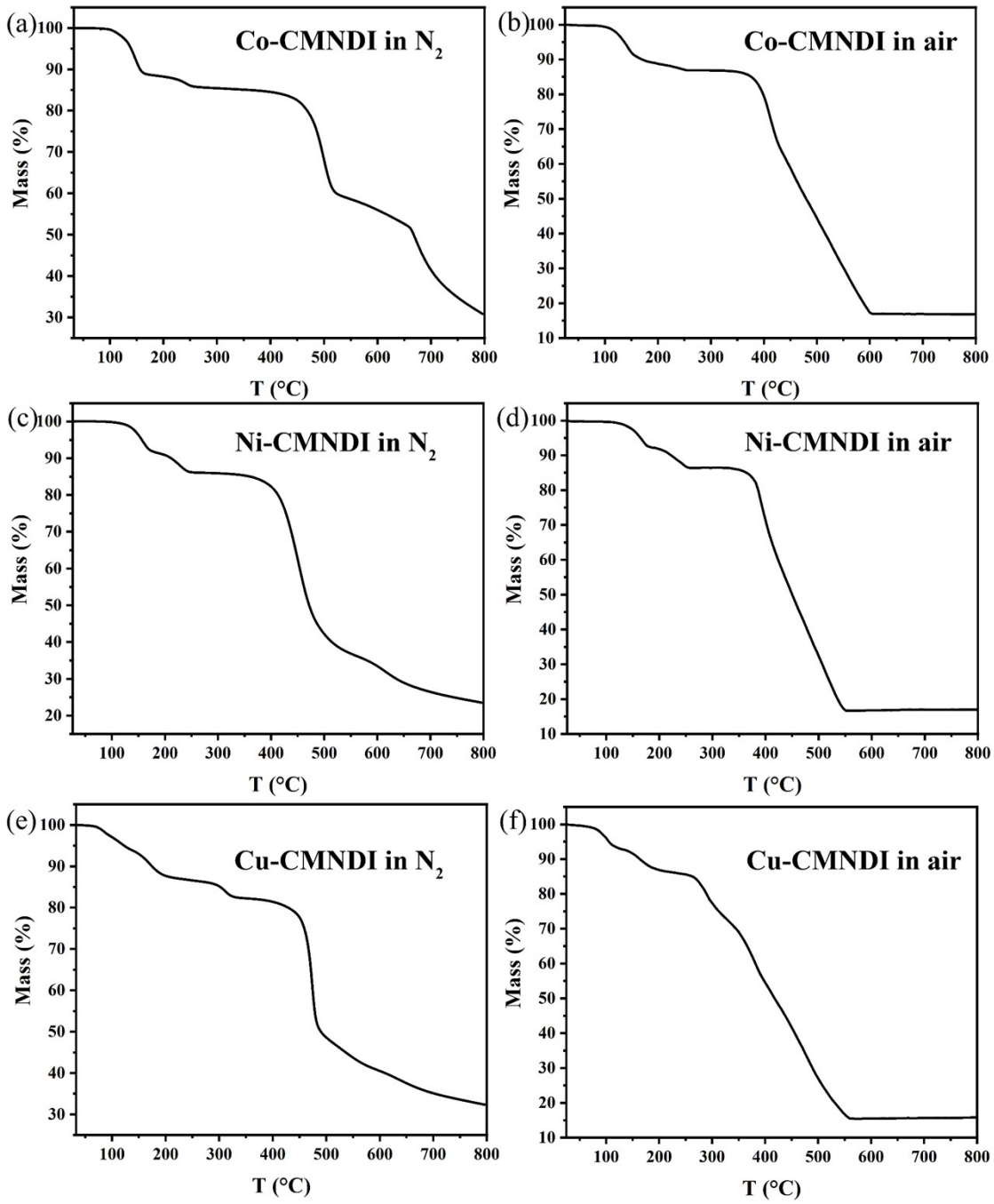

Figure S4. TG curves in N_2 atmosphere of Co-CMNDI (a), Ni-CMNDI (c), and Cu-CMNDI (e); TG curves in air atmosphere of Co-CMNDI (b), Ni-CMNDI (d), and Cu-CMNDI (f).

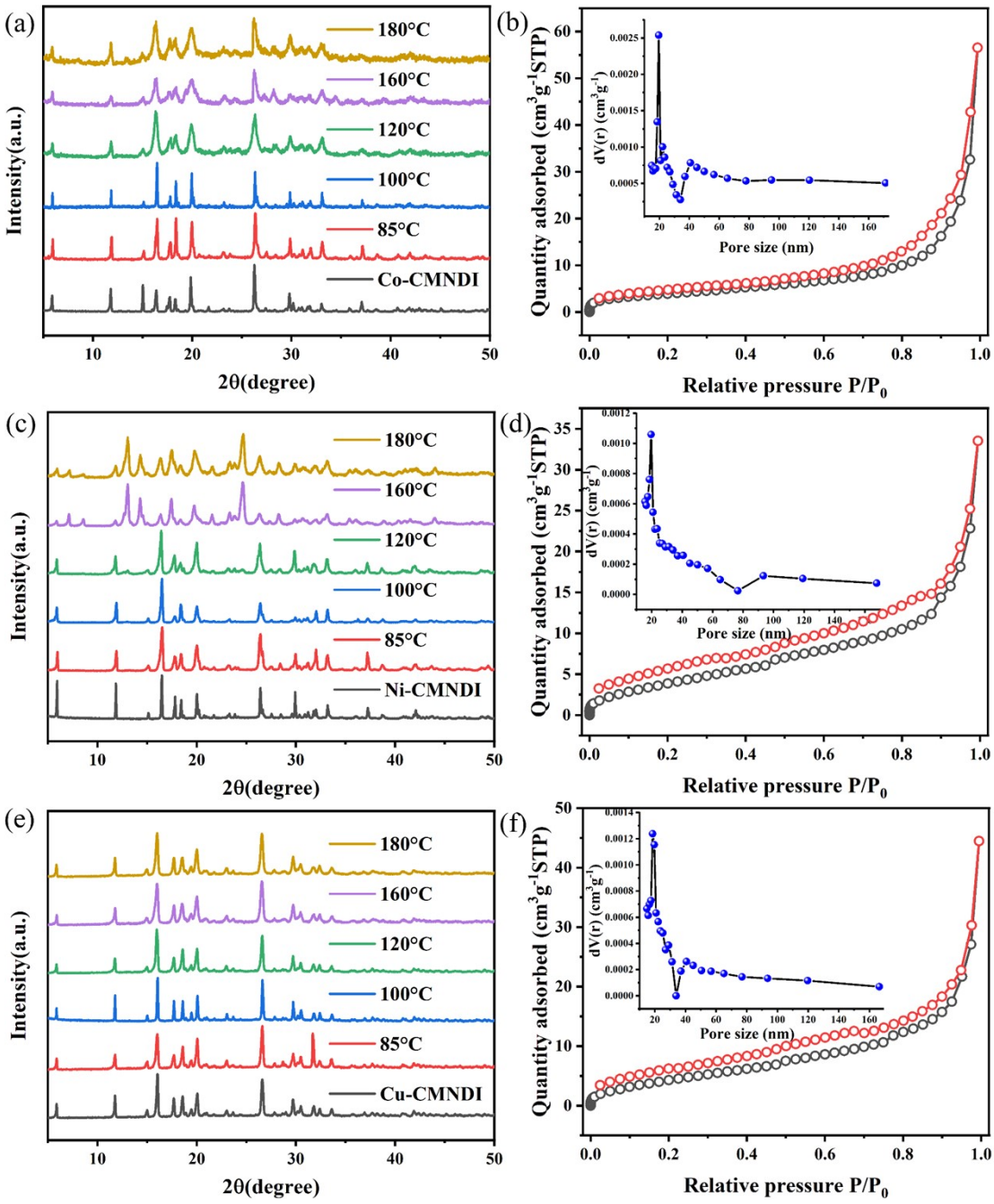

Figure S5. PXRD patterns at different temperatures of Co-CMNDI (a), Ni-CMNDI (c), and Cu-CMNDI (e); The N_2 adsorption–desorption isotherms and BJH pore size distribution curves (the insets) of Co-CMNDI (b), Ni-CMNDI (d), and Cu-CMNDI (f).

Table S4. Average R.G.B. values of time-dependent photochromic photos.

CNs	Co-CMNDI	Ni-CMNDI	Cu-CMNDI
0	(151, 116, 94)	(131, 126, 91)	(100, 138, 109)
0.5 h	(105, 81, 71)	(76, 68, 58)	(88, 105, 78)
1 h	(101, 79, 71)	(71, 65, 56)	(88, 103, 74)
1.5 h	(90, 70, 64)	(69, 63, 57)	(86, 100, 67)
2 h	(78, 60, 56)	(67, 62, 55)	(87, 96, 60)

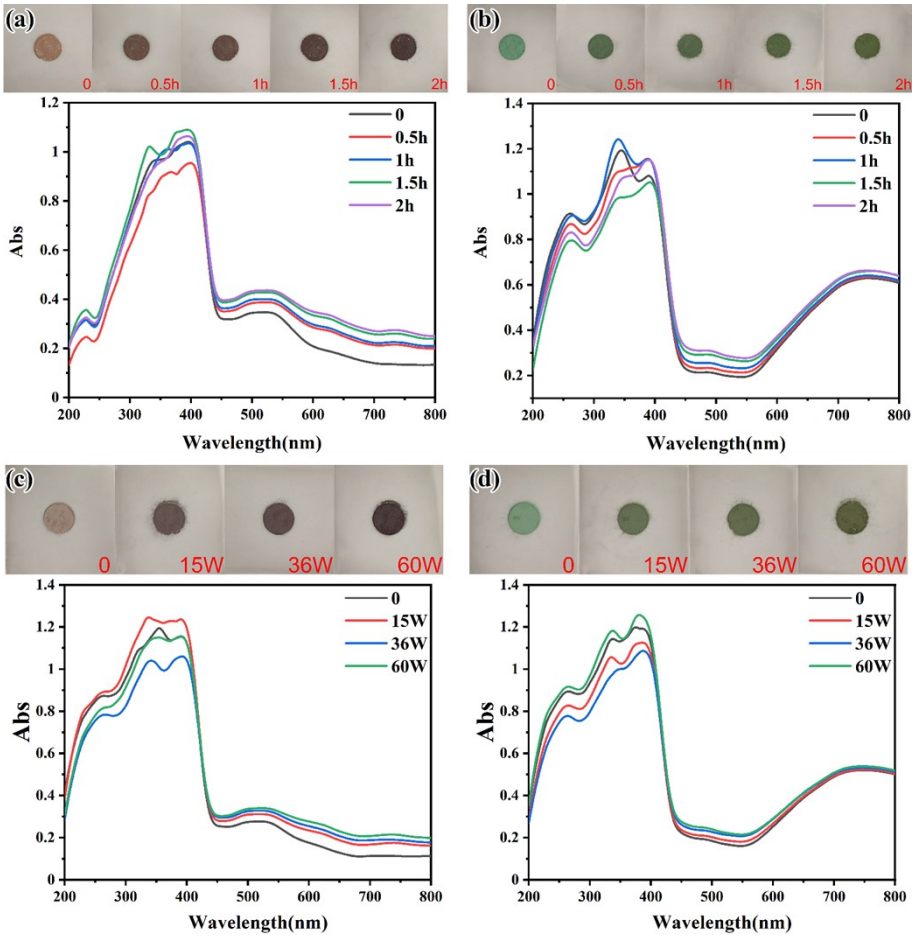

Figure S6. Time-dependent UV-vis spectra of Co-CMNDI (a) and Cu-CMNDI (b), power-dependent UV-vis spectra of Co-CMNDI (c) and Cu-CMNDI (d) and corresponding photochromic photos.

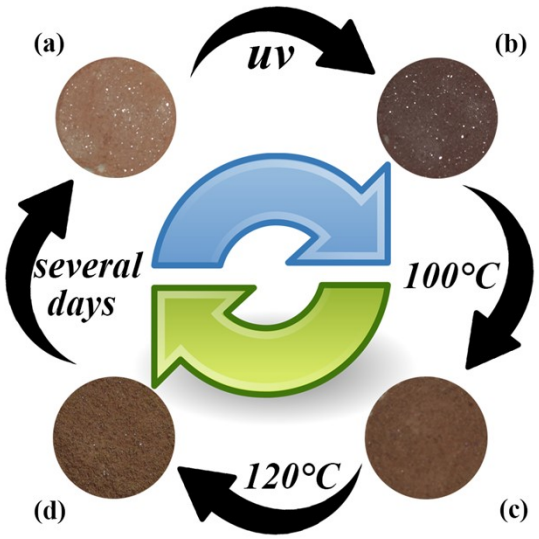

Figure S7. Photochromic reusability of Co-CMNDI: raw Co-CMNDI (a), after ultraviolet radiation (b), after being heated for 24 h at 100 °C (c), after being heated for 24 h at 120 °C (d).

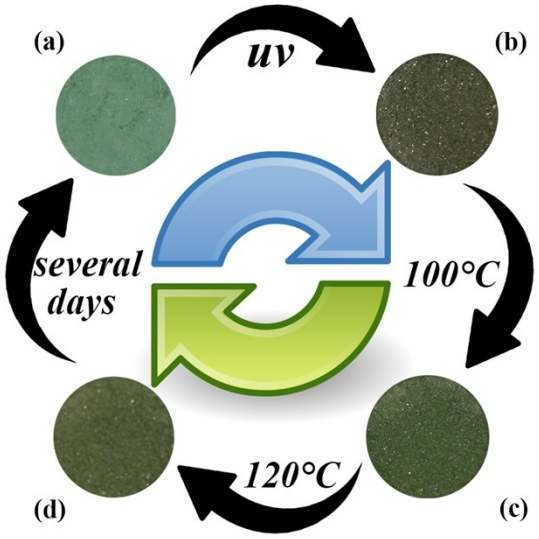

Figure S8. Photochromic reusability of Cu-CMNDI: raw Cu-CMNDI (a), after ultraviolet radiation (b), after being heated for 24 h at 100 °C (c), after being heated for 24 h at 120 °C (d).

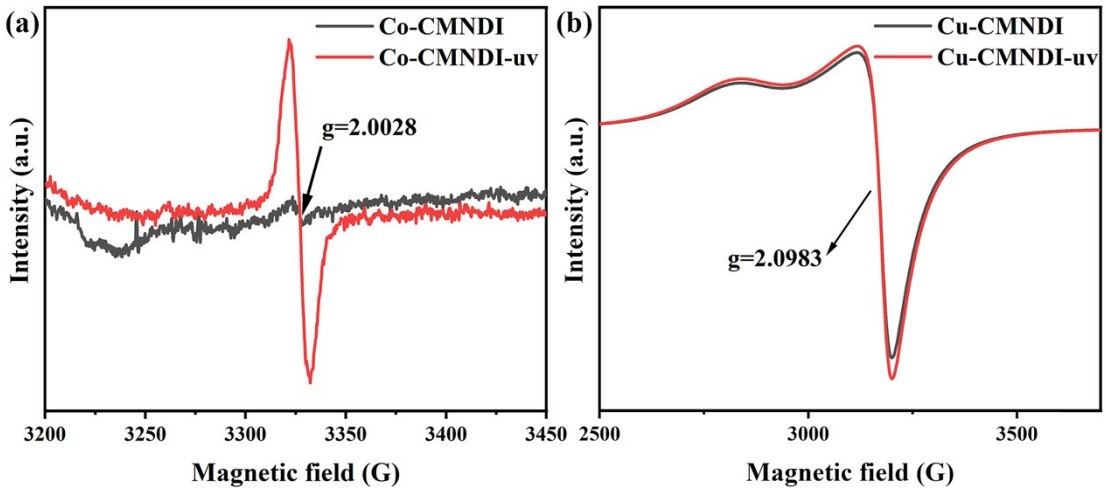

Figure S9. EPR spectra of as-synthesized Co-CMNDI and Co-CMNDI after ultraviolet radiation (a), as-synthesized Cu-CMNDI and Cu-CMNDI after ultraviolet radiation (b).

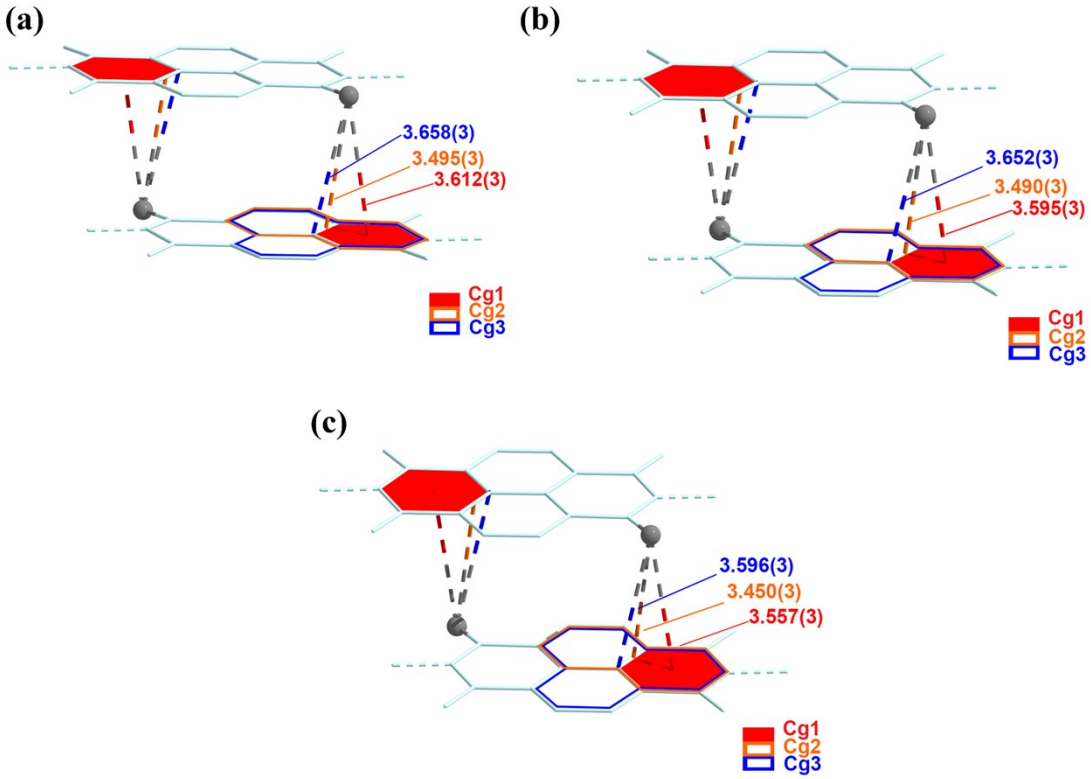

Figure S10. NDI cores of Co-CMNDI (a), Ni-CMNDI (b), and Cu-CMNDI (c) connecting through lone pair-π interactions (only NDI cores were shown for clarity).

Table S5. Lone pair-π interactions in Co-CMNDI*.

Y-X	Cg(J)*	X..Cg (Å)	Y-X..Cg (°)	Symmetry code(J)
C3-O5	Cg1	3.612(3)	105.7(2)	1+x, y, z
	Cg2	3.495(3)	88.3(2)	1+x, y, z
	Cg3	3.658(3)	93.5(2)	1+x, y, z

**Cg1: N1→C3→C4→C8_b→C7_b→C9_b→*

Cg2: N1→C3→C4→C8_b→C8→C4_b→C5_b→C6_b→C7_b→C9_b→

Cg3: N1→C3→C4→C5→C6→C7→C8→C4_b→C5_b→C6_b→C7_b→C9_b→

- Cg(J) = Center of gravity of ring J

- Y-X..Cg = Y-X-Cg angle (°)

- X..Cg = Distance of X to Cg (Å)

Table S6. Lone pair-π interactions in Ni-CMNDI*.

Y-X	Cg(J)	X..Cg (Å)	Y-X..Cg (°)	Symmetry code(J)
C4-O6	Cg1	3.595(3)	105.3(2)	-1+x, y, z
	Cg2	3.490(3)	87.89(19)	-1+x, y, z
	Cg3	3.652(3)	93.10(19)	-1+x, y, z

**Cg1: N1→C3→C5→C8→C6→C4→*

Cg2: N1→C3→C5→C7→C9_a→C6_a→C8_a→C8→C6→C4→

Cg3: N1→C3→C5→C7→C9_a→C6_a→C8_a→C5_a→C7_a→C9→C6→C4→

Table S7. Lone pair-π interactions in Cu-CMNDI

Y-X	Cg(J)	X..Cg (Å)	Y-X..Cg (°)	Symmetry code(J)
C9-O6	Cg1	3.557(3)	105.3(2)	1+x, y, z
	Cg2	3.450(3)	87.7(2)	1+x, y, z
	Cg3	3.596(3)	92.9(2)	1+x, y, z

Cg1: N5→C3→C4→C6→C8→C9→

Cg2: N5→C3→C4→C5→C7_b→C8_b→C6_b→C6→C8→C9→

Cg3: N5→C3→C4→C5→C7_b→C8_b→C6_b→C4_b→C5_b→C7→C8→C9→

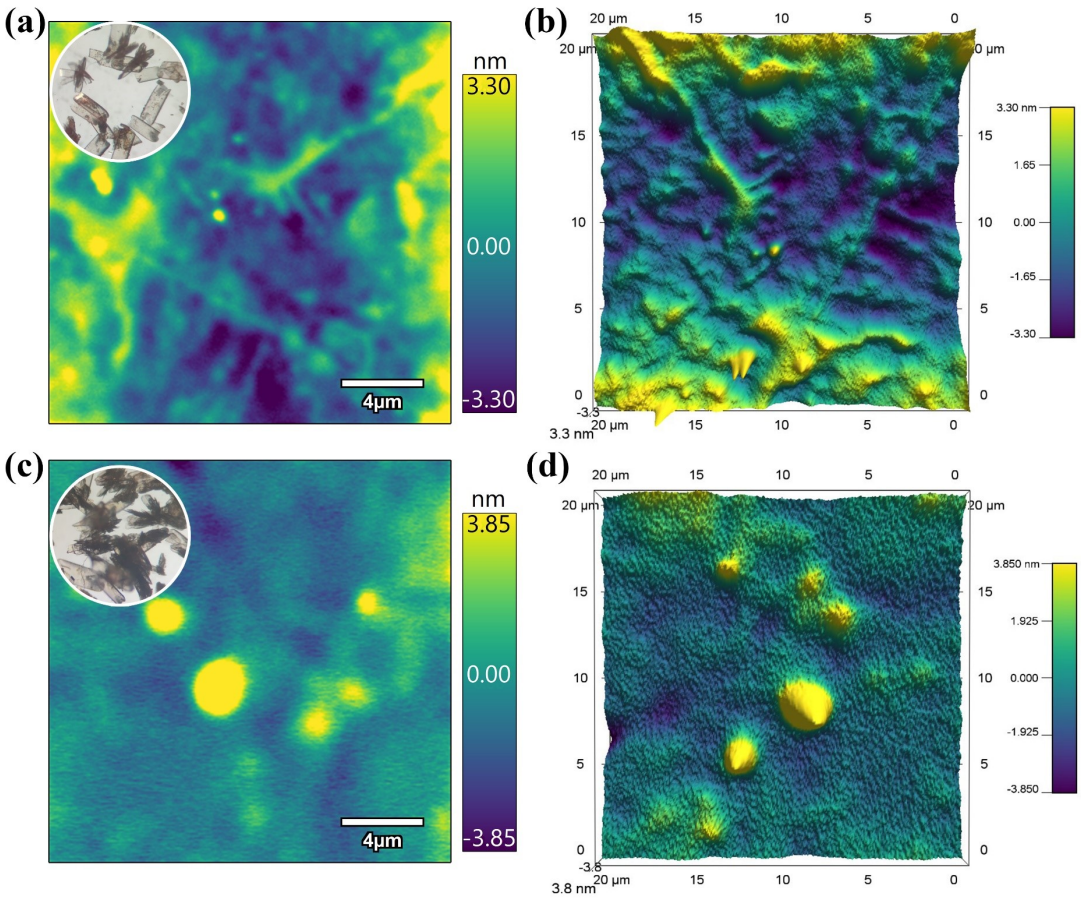

Figure S11. AFM images: height retrace image (a) and 3D view (b) of Co-CMNDI; height retrace image (c) and 3D view (d) of Co-CMNDI after ultraviolet radiation, insets are the corresponding photos under an optical microscope, all the AFM scan sizes were 20 μm × 20 μm.

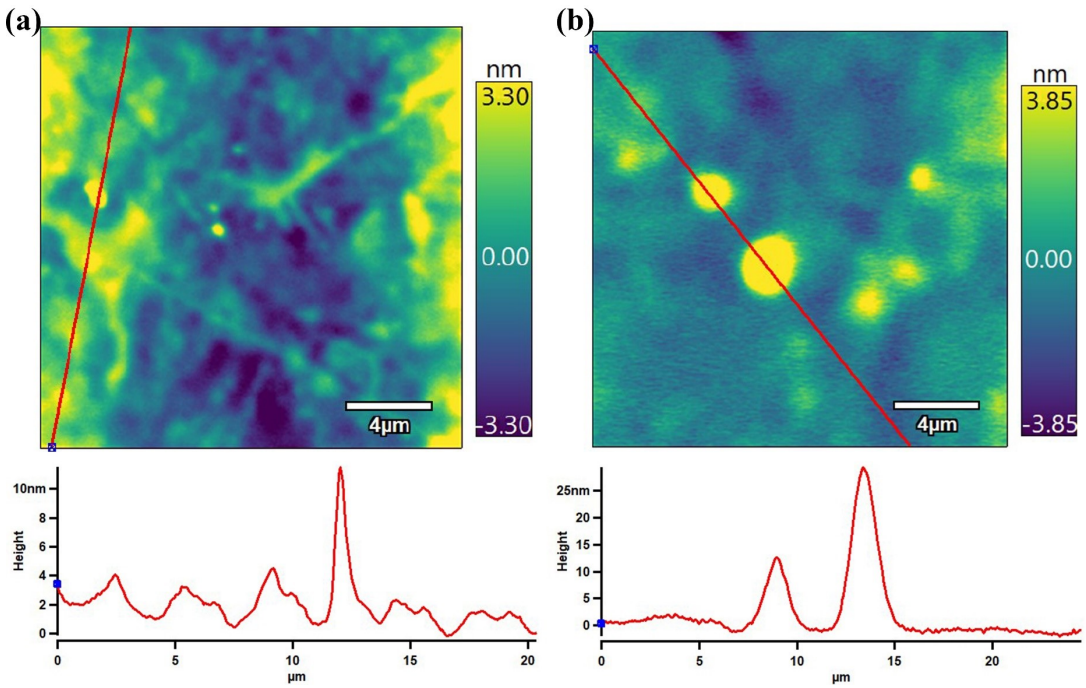

Figure S12. Selected AFM height profile charts of Co-CMNDI before (a) and after (b) ultraviolet radiation, all the AFM scan sizes were 20 μm × 20 μm.

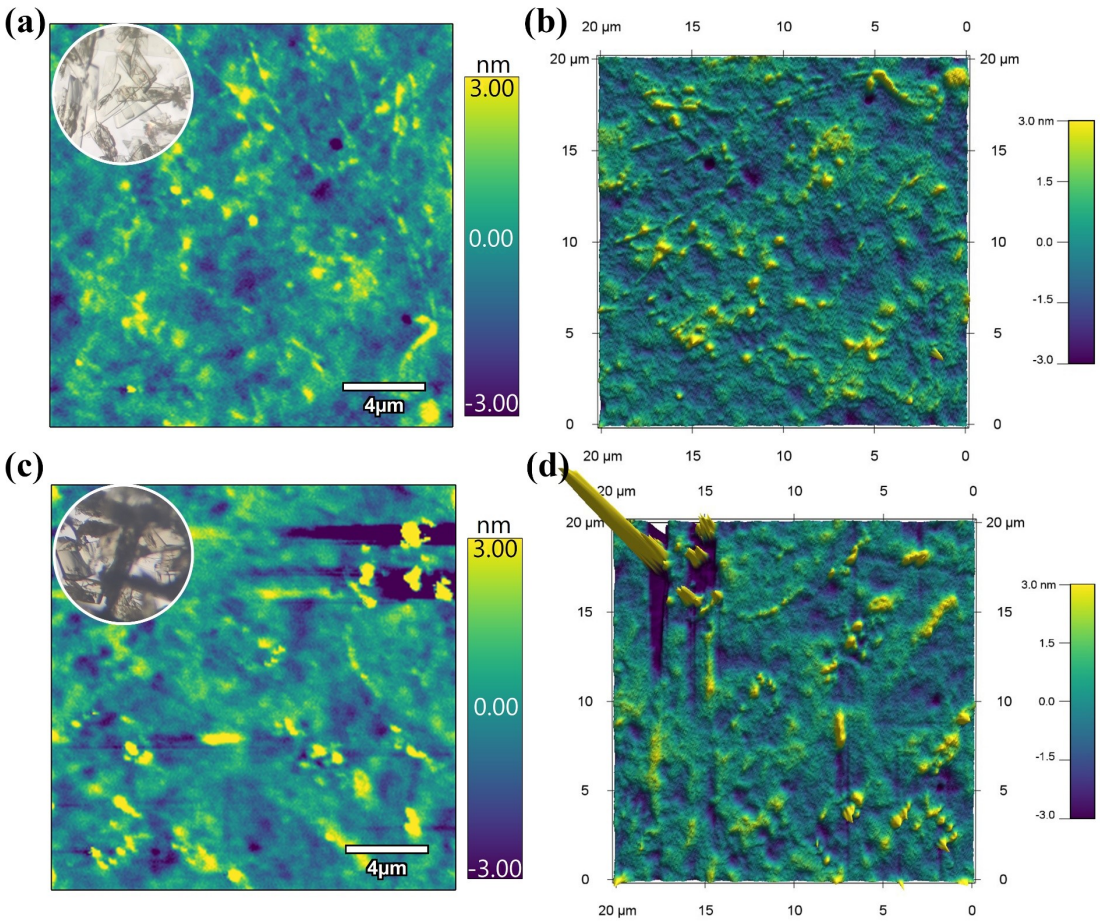

Figure S13. AFM images: height retrace image (a) and 3D view (b) of Ni-CMNDI; height retrace image (c) and 3D view (d) of Ni-CMNDI after ultraviolet radiation, insets are the corresponding photos under an optical microscope, all the AFM scan sizes were 20 μm × 20 μm.

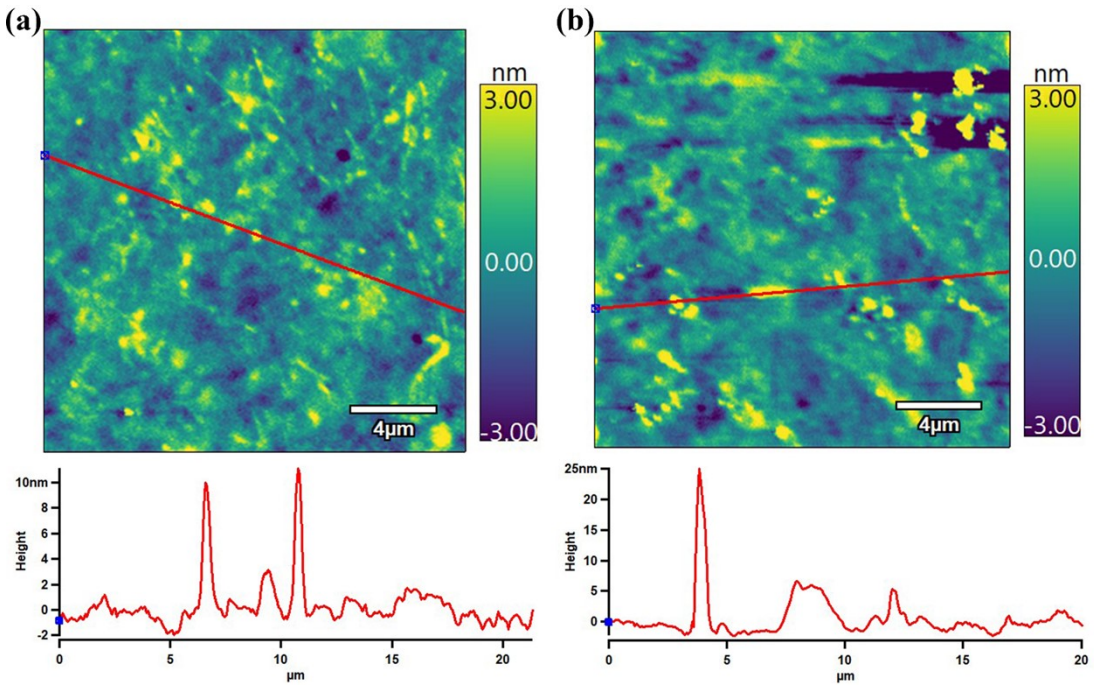

Figure S14. Selected AFM height profile charts of Ni-CMNDI before (a) and after (b) ultraviolet radiation, all the AFM scan sizes were 20 μm × 20 μm.

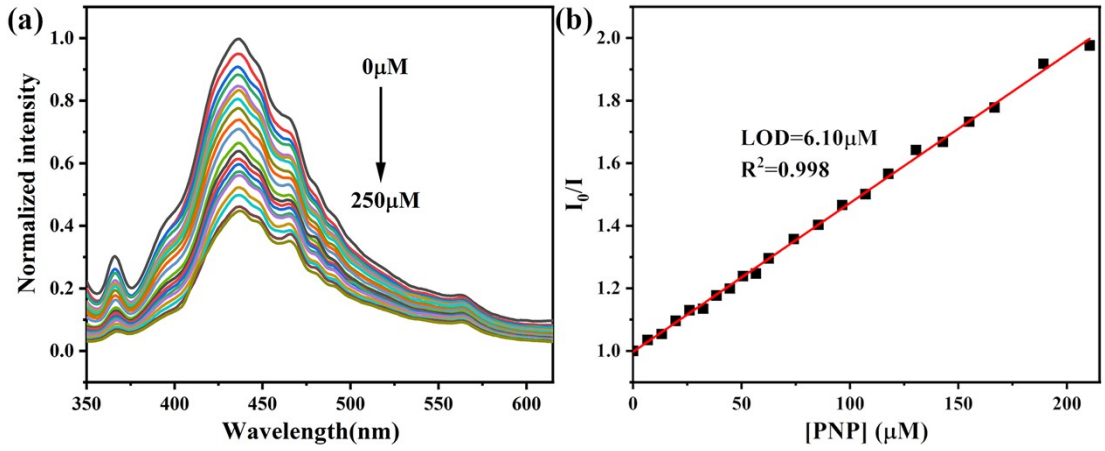

Figure S15. Fluorescence spectra of Cu-CMNDI with various concentrations of PNP (a), λ_{ex}=330 nm; Determination of Stern-Volmer quenching constant of PNP for the quenching of fluorescence of Cu-CMNDI (b).

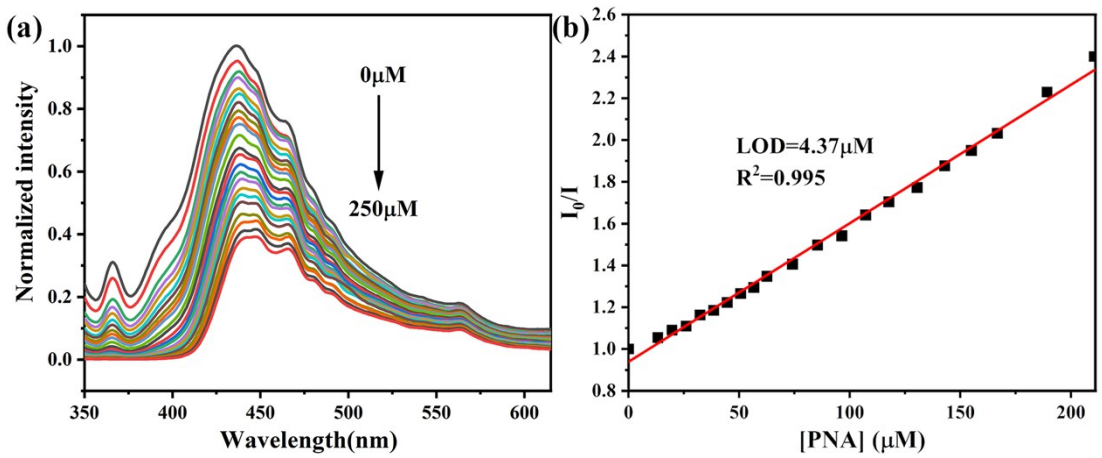

Figure S16. Fluorescence spectra of Cu-CMNDI with various concentrations of PNA (a), λ_{ex}=330 nm; Determination of Stern-Volmer quenching constant of PNA for the quenching of fluorescence of Cu-CMNDI (b).

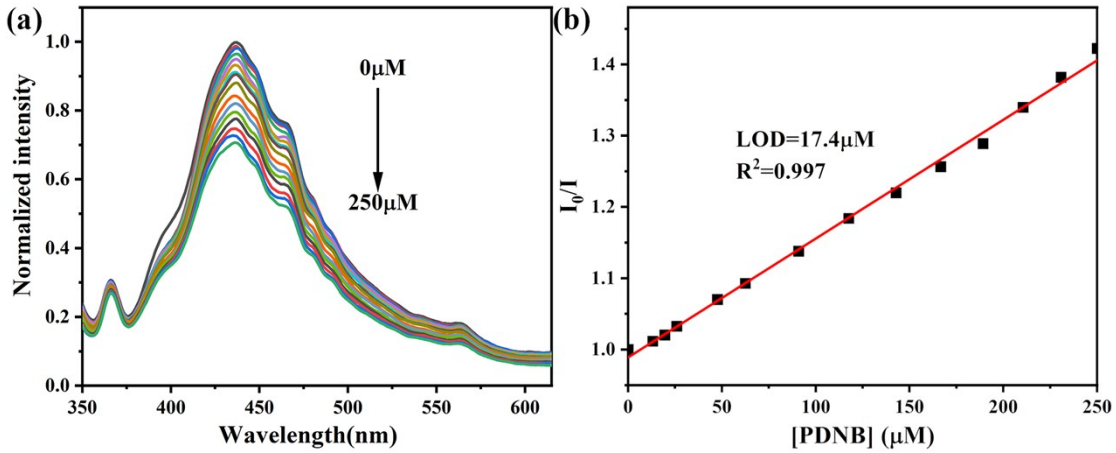

Figure S17. Fluorescence spectra of Cu-CMNDI with various concentrations of PDNB (a), λ_{ex}=330 nm; Determination of Stern-Volmer quenching constant of PDNB for the quenching of fluorescence of Cu-CMNDI (b).

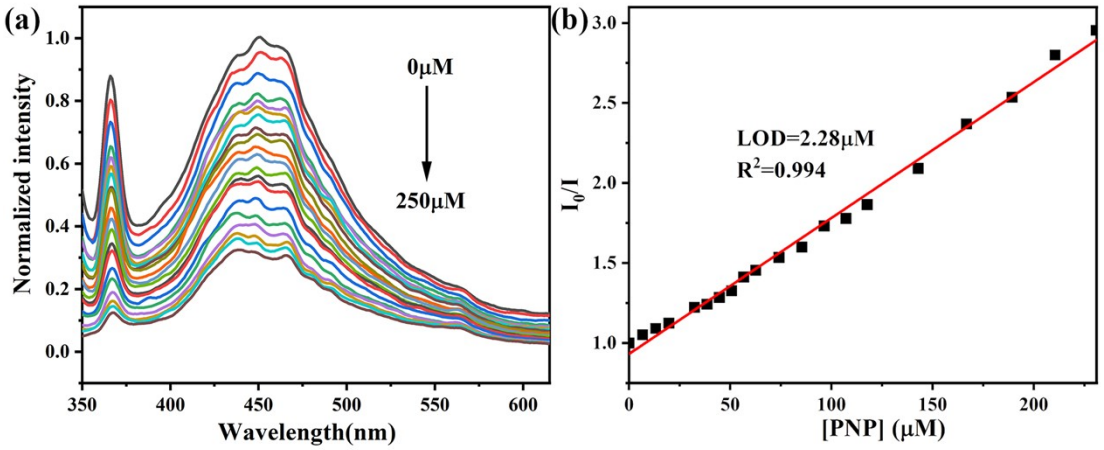

Figure S18. Fluorescence spectra of Ni-CMNDI with various concentrations of PNP (a), λ_{ex}=330 nm; Determination of Stern-Volmer quenching constant of PNP for the quenching of fluorescence of Ni-CMNDI (b).

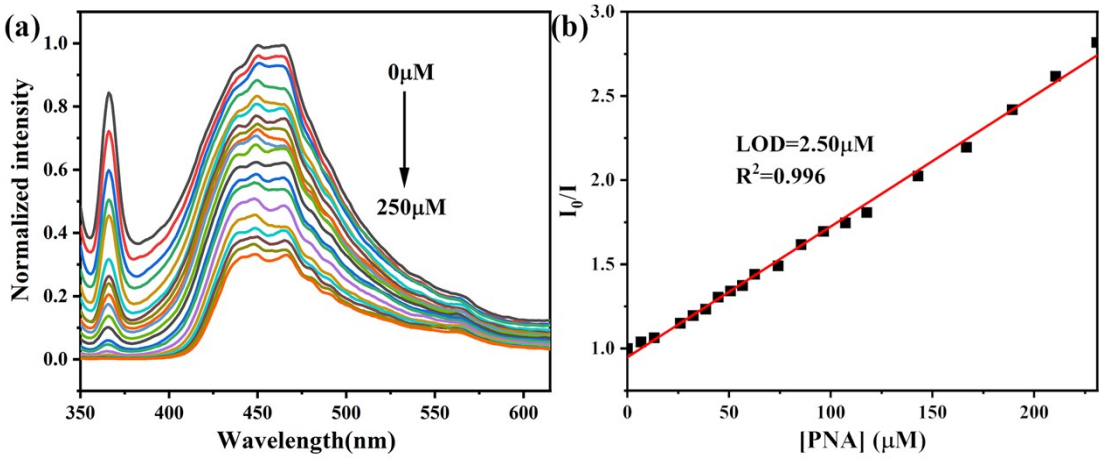

Figure S19. Fluorescence spectra of Ni-CMNDI with various concentrations of PNA (a), λ_{ex}=330 nm; Determination of Stern-Volmer quenching constant of PNA for the quenching of fluorescence of Ni-CMNDI (b).

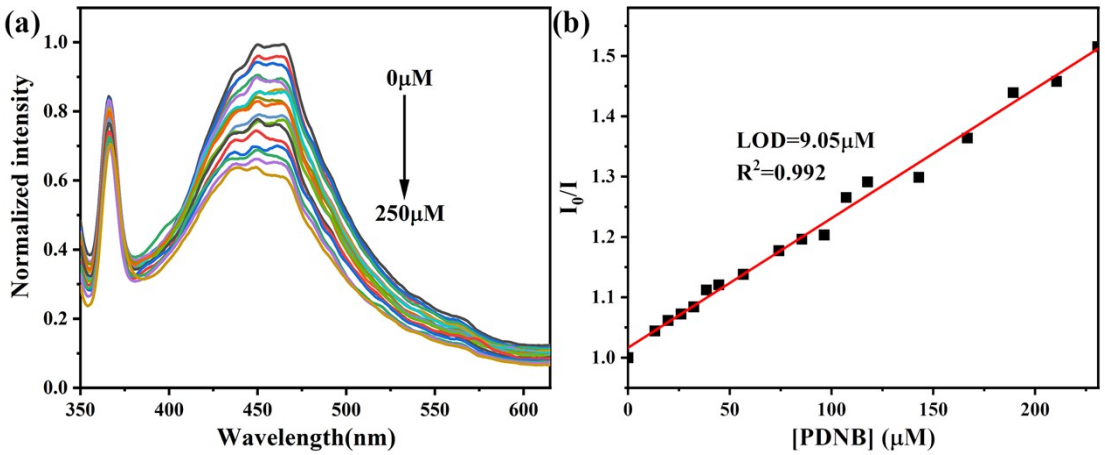

Figure S20. Fluorescence spectra of Ni-CMNDI with various concentrations of PDNB (a), λ_{ex}=330 nm; Determination of Stern-Volmer quenching constant of PDNB for the quenching of fluorescence of Ni-CMNDI (b).

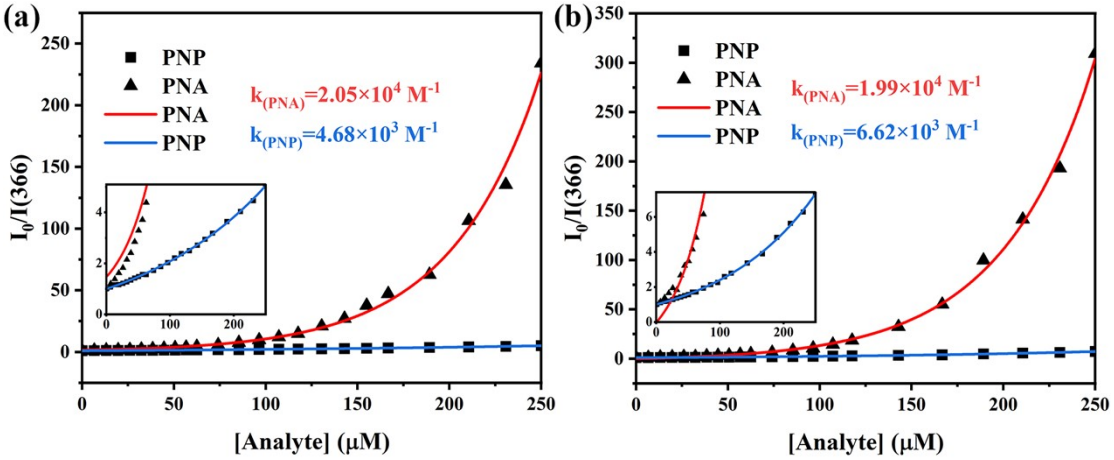

Figure S21. Nonlinear Stern-Volmer equation fitting of Cu-CMNDI (a) and Ni-CMNDI (b) towards PNA and PNP (λ_{em}=366 nm), inset only changes the ordinate of the fitting curve.

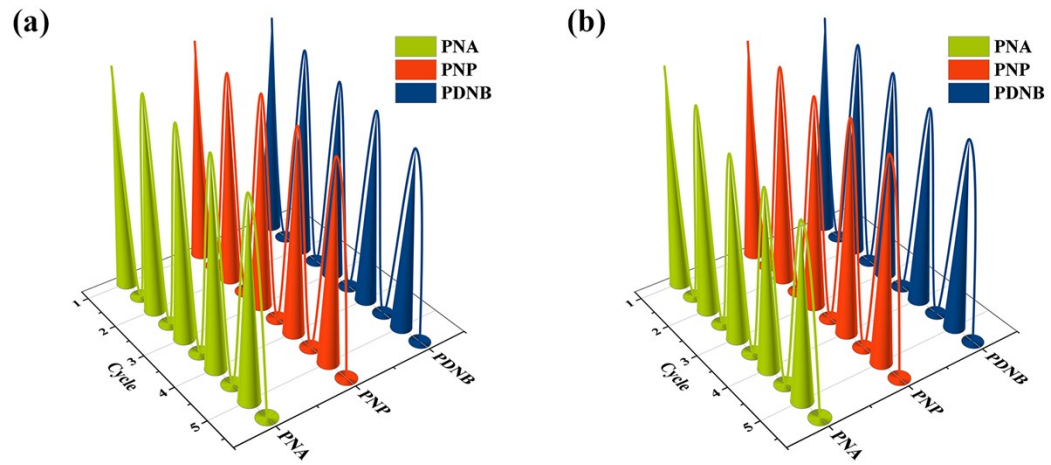

Figure S22. Fluorescence intensities of Cu-CMNDI (a) or Ni-CMNDI (b) towards nitroaromatics in five cycles experiments.

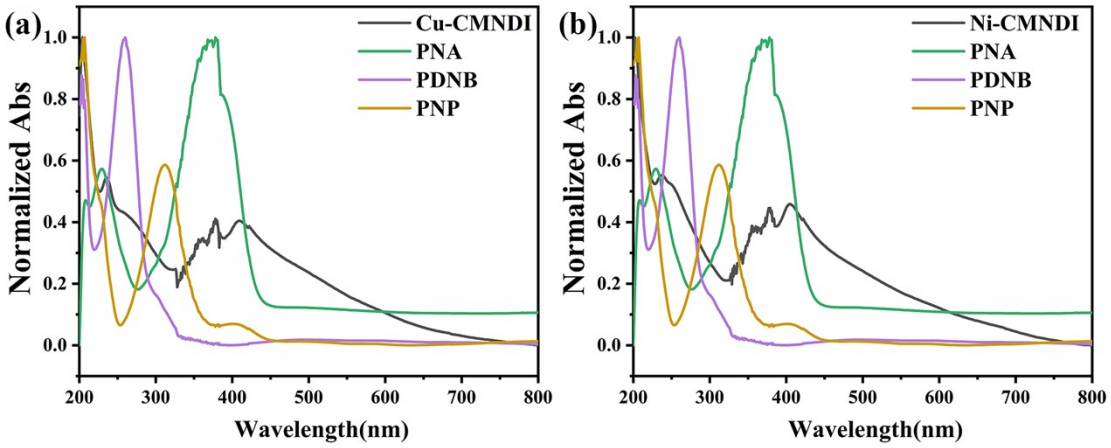

Figure S23. Overlap of absorption spectra of Cu-CMNDI (a), Ni-CMNDI (b) and nitroaromatics analytes.

Table S8. HOMO, LUMO energies, and HOMO-LUMO gap of CMNDI, CMNDI*, and analyzes.

	HOMO/eV	LUMO/eV	HOMO-LUMO gap/eV
CMNDI	-7.17	-3.546	3.624
CMNDI*	-0.941	1.689	2.630
PNP	-6.921	-2.222	4.699
PNA	-6.253	-1.955	4.298
PDNB	-8.349	-3.495	4.854

References

1. C. F. Macrae, I. J. Bruno, J. A. Chisholm, P. R. Edgington, P. McCabe, E. Pidcock, L. Rodriguez-Monge, R. Taylor, J. Streek and P. A. Wood, *J. Appl. Crystallogr.*, 2008, **41**, 466-470.
2. G. M. Sheldrick, *Acta Crystallogr. A*, 2008, **64**, 112-122.
3. A. L. Spek, *J. Appl. Crystallogr.*, 2003, **36**, 7-13.
4. M. J. Frisch, G. W. Trucks, H. B. Schlegel, G. E. Scuseria, M. A. Robb, J. R. Cheeseman, G. Scalmani, V. Barone, B. Mennucci, G. A. Petersson, H. Nakatsuji, M. Caricato, X. Li, H. P. Hratchian, A. F. Izmaylov, J. Bloino, G. Zheng, J. L. Sonnenberg, M. Hada, M. Ehara, K. Toyota, R. Fukuda, J. Hasegawa, M. Ishida, T. Nakajima, Y. Honda, O. Kitao, H. Nakai, T. Vreven, J. A. Montgomery Jr., J. E. Peralta, F. Ogliaro, M. J. Bearpark, J. Heyd, E. N. Brothers, K. N. Kudin, V. N. Staroverov, R. Kobayashi, J. Normand, K. Raghavachari, A. P. Rendell, J. C. Burant, S. S. Iyengar, J. Tomasi, M. Cossi, N. Rega, N. J. Millam, M. Klene, J. E. Knox, J. B. Cross, V. Bakken, C. Adamo, J. Jaramillo, R. Gomperts, R. E. Stratmann, O. Yazyev, A. J. Austin, R. Cammi, C. Pomelli, J. W. Ochterski, R. L. Martin, K. Morokuma, V. G. Zakrzewski, G. A. Voth, P. Salvador, J. J. Dannenberg, S. Dapprich, A. D. Daniels, O. Farkas, J. B. Foresman, J. V. Ortiz, J. Cioslowski, D. J. Fox, Gaussian, Inc., Wallingford, CT, USA, 2009.